Poly(ethylene terephthalate) Fibers. 1. Crystal Structure and Morphology Studies with Full-Pattern X-ray Diffraction Refinement

Yigang Fu,[†,‡] William R. Busing,[‡] Yimin Jin,[†,‡] Kathleen A. Affholter,[§] and Bernhard Wunderlich*[,†,‡]

Department of Chemistry, University of Tennessee, Knoxville, Tennessee 37996-1600, Chemistry Division of Oak Ridge National Laboratory, Oak Ridge, Tennessee 37831-6197, and Chemical Technology Division of Oak Ridge National Laboratory, Oak Ridge, Tennessee 37831-6194

Received October 22, 1992; Revised Manuscript Received January 19, 1993

ABSTRACT: Full-pattern fiber X-ray diffraction refinement has been used to study the structure and morphology of the crystallites of three poly(ethylene terephthalate) fiber samples with different heat treatment history. Diffraction data over the whole two-dimensional space were collected with a four-circle diffractometer. An iterative Fourier filter method is developed to separate the crystalline diffraction from the background scattering. Both the structure and morphology are found to be dependent on the heat treatment. Some properties of the fibers can be explained by the difference in the crystal structure and morphology of crystallites.

Introduction

Most polymer fibers of practical importance are semicrystalline. The crystallites of the fibers are aligned in only one dimension, approximately parallel to the fiber axis direction. Otherwise the orientation of the crystallites is totally random. This one-dimensional orientation results in a cylindrical symmetry of the fiber diffraction patterns. The presence of this cylindrical symmetry makes the fiber diffraction patterns two-dimensional. The cylindrical average causes overlap for some reflections and weakens the intensities for the reflections which are not located at the fiber axis. The size of the crystallites in fibers is usually on the order of 10 nm or less. In addition, more defects are expected in the crystallites than in the single crystals of small molecules. The small size of the crystallites and the presence of defects broaden the reflection peaks and make the overlap worse. In the traditional fiber diffraction studies, each reflection is represented by only one point. However, there are usually not enough isolated reflections for a full structure analysis. Furthermore, the nonlinear background scattering can, in most positions of data collection, be more intense than the crystalline diffraction and needs to be removed from the observed fiber diffraction data before a reliable structure analysis becomes possible.

The recent development of the full-pattern (two-dimensional Rietveld) fiber refinement method[1-6] overcomes some of the just-described disadvantages. In this new approach each reflection is represented by one fully characterized peak. Therefore, not only the crystal structure but also the morphology of the crystallites can be assessed by two-dimensional profile fitting of all diffraction peaks. A full-pattern refinement computer program, FIBLS, which has been developed by Busing[5] in this laboratory is used in this study. A brief summary of the program can be found in ref 5. A detailed description of the program, FIBLS, will be published in a separate paper. A model of the structure of the crystallites is first used to calculate a three-dimensional diffraction pattern. The three-dimensional, calculated diffraction pattern is then rotated to produce a two-dimensional, calculated diffraction pattern which is compared to the two-dimensional, observed fiber diffraction pattern at each point of the data collection. The structure model chosen includes parameters which define the morphology and the crystal structure of the crystallites. The full complement of parameters used in the refinement are the average size of the crystallites in three dimensions, the distribution of disorientation of the crystallites relative to each other (the mosaic distribution), the average orientation of the crystallites with respect to the fiber axis, a scale factor, the unit-cell parameters, the atomic positions (usually determined using a rigid-body model), a temperature factor, a paracrystallinity matrix for the defects, and the parameters of the diffractometer. A four-circle diffractometer was used to collect the accurate diffraction intensities to high scattering angles.

The crystal structure of poly(ethylene terephthalate) (hereafter, PET) fibers has been extensively studied with X-ray or electron diffraction methods since the early 1950s.[7-13] The accuracy of these previous diffraction studies is limited by the traditional integrated intensity refinement method and is also limited by the quality of data collection by the photographic techniques. In this paper the results of studies of three PET fiber samples are reported. These three fiber samples differ only in heat treatment. The purpose of this project was to precisely determine and discuss the structure and morphology of the crystallites of polymer fibers, to study change of the structure and morphology with heat treatment, and to investigate the relation between fiber properties and the features of the crystallites. Besides the here reported measurements, small-angle X-ray scattering (SAXS), differential scanning calorimetry (DSC), thermal mechanical analysis (TMA), and atomic force microscopy (AFM) were also used to study the same PET fiber samples. The detailed description of these results will be reported in the future. The results from full-pattern X-ray diffraction will be compared with initial results from these other techniques.

Experiment

The basic PET fiber sample, named PET4, was provided by Dr. G.-Y. Chen.[14] The fiber was a typical fiber with an intrinsic viscosity of 0.95 dL/g. It was spun with a take-up speed of 4000 m/min. Two other samples have been made from the PET4

[†] University of Tennessee.
[‡] Chemistry Division of Oak Ridge National Laboratory.
[§] Chemical Technology Division of Oak Ridge National Laboratory.

0024-9297/93/2226-2187$04.00/0

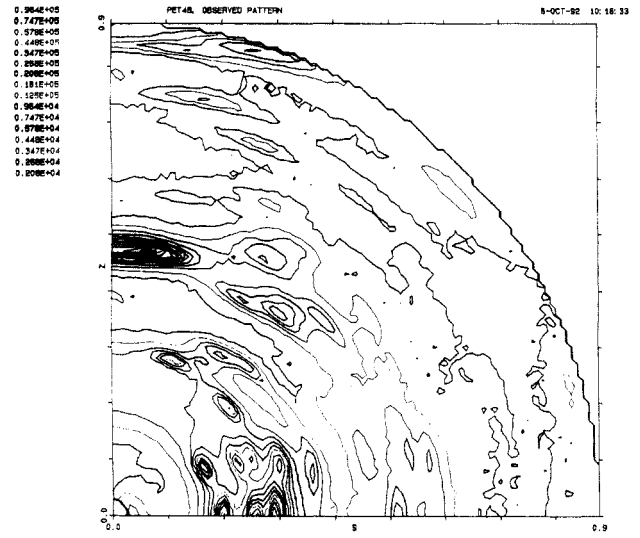

Figure 1. Contour plot of the observed diffraction intensity pattern of PET4B in reciprocal space. The values of the contours are listed in the top left corner of this figure. The interval of the contours is $(0.1)^{1/9}$ of the value of the previous contour line. The unit in both axes s (equator) and z (meridian) is Å^{-1}. Data collection limit is $(s^2 + z^2)^{1/2} \leq 0.88$ Å^{-1}.

fibers. Annealing of the fiber with its ends fixed at 200 °C for about 84 h in nitrogen led to sample PET4A. Annealing under tension at the same temperature and for the same time as PET4A led to sample PET4B. The tension in the latter annealing was applied by wrapping individual fibers on a compressed U-shaped plate spring. The exact magnitude of the tension was not measured. The diameter of an individual fiber is about 15 μm. The aligned fibers were coated with a dilute collodion solution which dried to make a stiff 1.5-mm bundle. The fiber bundle was then mounted on a goniometer of the Huber four-circle diffractometer, and the fiber axis aligned optically along the ϕ axis. Cu Kα X-rays were used with a graphite monochromator. A 4-mm square counter aperture was located 28 cm from the sample. All data were collected at room temperature.

Scattering was measured in the bisecting mode by setting the diffractometer angles χ, ω, and 2θ. A total of 89 scans were made parallel to the layer lines at z values from 0.0 to 0.88 Å^{-1} at intervals of 0.01 Å^{-1} in reciprocal space. For each scan individual counts were measured for 240 s in steps of 0.01 Å^{-1} from 0.0 to 0.88 Å^{-1} in reciprocal space. Measurements were made at each point on this two-dimensional grid for which $2° \leq 2\theta \leq 86°$. A standard count was measured every 80 min to verify that there was no significant intensity change during data collection. A contour plot of the observed diffraction intensity patterns of PET4B is depicted in Figure 1. The equatorial and meridional axes are labeled s and z, respectively.

Background Scattering Correction

It is clearly seen from Figure 1 that there is considerable scattering intensity everywhere within the range of the data collection. All contributions to the observed intensities not attributable to the diffraction of the crystalline material are regarded as background in this paper. The diffraction pattern as seen in Figure 1 cannot be directly used for structure refinement because of the high proportion of background scattering. The separation of the background from the crystalline diffraction is, thus, a core problem for full-pattern refinement in fiber diffraction.[6]

The background includes the noncrystalline material scattering, Compton scattering, thermal diffuse scattering, and the scattering from defects.[15] The PET fiber samples include large amounts of noncrystalline (amorphous) material. It has been recognized that part of this amorphous phase in PET fibers may show significant orientation.[16-20] This orientation of the amorphous phase may lead to both sharp diffraction peaks and diffuse scattering. The background either can be removed before refinement or can be represented by suitable functions which can be taken into account in the calculated pattern. Even though the second method has the advantage of avoiding any manipulation of observed data, the first method had to be used in this work because of the complexity of the background caused by orientation of the amorphous phase. This complexity did not permit us to find as suitable functions to represent the background sufficiently well.

An iterative Fourier filter method was developed in this study to remove the background from the diffraction pattern. This Fourier filter method was derived from the method described earlier by Richardson and Faber.[21] It is based on the intrinsic difference of the background scattering from the crystalline diffraction. The background scattering usually varies, in the same region, less than the crystalline reflections. The difference in the distribution patterns of the Fourier transformation of a sharp peak and a broad peak or relatively flat curve can then be used to separate the sharp peaks from the background. Further treatment of the noncrystalline material is described in part 2 of this series of publications.

A Fourier transformation converts a data set to the frequency domain. The transformation of a constant background consists of a single peak at zero frequency. The transformation of relatively flat curves or broad peaks is concentrated in the low-frequency region, and the amplitude of its oscillations declines rapidly. The flatter the curves, the narrower the frequency range and the more rapidly does the outline of the amplitudes decline. On the other hand, the Fourier transformation of a sharp peak ranges from low to high frequency and the amplitude of its oscillations declines slowly. The sharper the peaks, the farther extends the distribution of the Fourier transformation pattern.

In order to separate the background, we first make a Fourier transformation of the intensity data set. We multiply this transformation by a suitable modifying function to retain the low-frequency part of the pattern. A back Fourier transformation of this low-frequency pattern can be assumed to approximate the background. Subtraction of this background from the original diffraction pattern results in an approximate crystalline diffraction pattern that can be used in structure refinement. This whole procedure is called a Fourier filter.

The intensities of the strongest reflections, however, are much higher than the remaining part of the observed diffraction pattern. This makes it difficult to find a modifying function that can satisfactorily remove the background without also deleting the weak crystalline reflection peaks. After the first cycle of the background correction only the strong crystalline reflection peaks are likely to remain. The intensities and the shapes of these strong peaks may also be distorted by the background correction, and a structure model based on these data alone would contain errors. To improve the structure model, we compute a difference pattern between the original diffraction pattern and the preliminary, calculated diffraction pattern. This difference represents the background and the residuals. The residuals are positive and negative peaks of much lower intensities than the strong peaks. Next we let the difference pattern pass through the Fourier filter, resulting in minimization of some of the residuals. The thus generated background based on the second cycle of corrections is closer to reality, and a better structure model can be obtained from this refinement. A further difference pattern shows that the amplitudes of

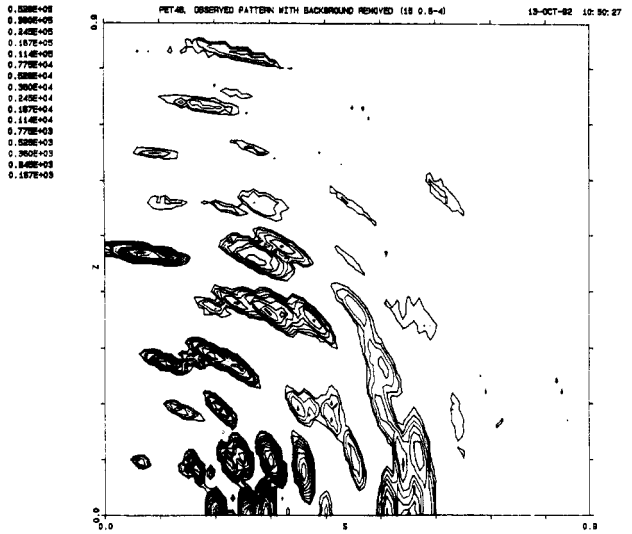

Figure 2. Contour plot of the observed crystalline diffraction intensity pattern of PET4B after final background removal. The interval of the contours is $(0.1)^{1/6}$ of the value of the previous contour line. The Tukey modifying function parameters are 15, 0.8, and 4.0 for Δs, r_1 and r_2, respectively.

the residuals are now considerably reduced. A satisfactory background can be generated by further iterating the Fourier filter method with the successive difference patterns. In the present work typically five to six iterations were used.

In this study a one-dimensional Fourier transformation was made to each layer of the original or difference pattern using a fast Fourier transformation method. A Tukey function[22] was chosen as a modifying function. The cut-off range was increased with each cycle of the background correction. Figure 2 shows the PET4B crystalline diffraction pattern with the background removed as it was used in the final full-pattern refinement.

Structure Refinement

All structure refinements were done by using the program FIBLS. The first full-pattern refinement was based on the data from PET4B. The final results of this were then used as starting parameters for the refinement of PET4A and PET4. The refinement was separated into four steps, because varying all parameters in the beginning of a refinement usually causes it to diverge. Each step of refinement was performed only after the refinement of the previous step had converged. Data points with intensities less than a specified small value were not included in the refinement.

In the first step only the unit-cell parameters and the molecular chain direction vector were varied. The latter defines the angle of tilt between the molecular chains or the c-axis of the crystallites and the fiber axis. The positions of the crystalline reflection peaks depend on these parameters. Initial values were taken from Daubeny, Bunn, and Brown (hereafter DBB).[7] A preliminary refinement was made by using a general least-squares program to fit the observed positions of a few isolated reflections to which indices could be assigned. These results were refined further using the program FIBLS. The initial dimensions of crystallites were preset at 100 Å, and the paracrystallinity parameters were all taken as zero. A scale factor was always included in the variables.

As a second step, parameters that determine the shape of the reflection peaks were varied. These quantities are the crystalline disorientation, size, and paracrystallinity.[23] To reduce the number of these parameters, it is assumed that the crystallites have rotational symmetry about the fiber axis. Arbitrary intensities for 15 strong nonoverlapping reflections were included as variables for the initial determination of these peak-shape parameters.

The molecular structure was varied in the third step. The parameters include the interatomic bond lengths, angles, conformation angles, molecular orientation angle, and temperature factors. The orientation angle is the angle between the ac-plane and the plane that contains the O1–C1–C1′–O1′ atoms. These parameters determine the intensities of the reflections. A rigid-body model was used to reduce the number of variables. The values of the bond lengths and angles were preset according to the reported dimethyl terephthalate[24] and ethylene glycol bis(p-chlorobenzoate)[25] structures. The conformation angle C3–C2–O1–C1 was first adjusted to satisfy the condition that the distance between the middle point of the C1–C1′ bond and the center of the benzene ring must be equal to $^1/_2$ of the length of the c axis. The other two conformation angles, C2–O1–C1–C1′ and C4–C3–C2–O1, and the molecular orientation angle ψ were then refined. The bond lengths and angles were added into the variables when the previous refinements converged. The H atoms were added into the structure with a fixed C–H bond length of 1.0 Å. The C–C bond length and C–C–C and H–C–C angles of the benzene ring were always fixed at 1.39 Å and 120°, respectively. For PET4, only the conformation angles and the molecule orientation angle were refined. All the bond length and angle values were fixed at values from the results of the PET4B refinement. The temperature factor was constrained to be isotropic for all atoms. The Bragg temperature factor of H atoms was 1 Å^2 larger than that of the C atoms.

Finally, all the parameters which varied separately in the previous steps were refined simultaneously. High correlation coefficients appeared between the scale factor and some parameters of the molecular structure and between the scale factor and the crystallite sizes. The results of this final refinement step are given in Table I. Atomic coordinates are listed in Table II. Interatomic bond lengths, bond angles, and conformation angles are given in Table III. The results of DBB's study[7] are also included in Table III for comparison. The configuration of the PET4B molecule and the arrangement of the molecules in the crystal are shown in Figures 3 and 4, respectively. A contour plot of the calculated intensity pattern of PET4B is shown in Figure 5.

Discussion

All diffraction peaks which are recognizable in the original observed pattern (Figure 1) can be found in the calculated diffraction pattern (Figure 5). The positions and shapes of these diffraction peaks match fairly well in both figures. Because of the presence of the noncrystalline material, expecially the oriented noncrystalline material, the difference pattern between the observed and calculated patterns not only represents the error of the structure model but also represents the noncrystalline diffraction. In some regions the latter may be much stronger than the former. The difference pattern, therefore, is used in the second paper of this series to analyze the noncrystalline material structure. It should be pointed out that the agreement factors which are listed in Table I measure only the agreement between the calculated intensities and the observed intensities *after* background correction. These values are also not equivalent to those in other crystallographic studies of integrated intensity refinement because the number of observations is not the same as the

Table I
Final Parameters of the PET Crystal Model after Full-Pattern Refinement

	PET4	PET4A	PET4B
space group: $P\bar{1}$, $Z = 1$			
X-ray wavelength: 1.5418 Å			
a (Å)	4.5609 (5)	4.5221 (2)	4.5087 (2)
b (Å)	5.9531 (5)	5.9214 (2)	5.8818 (3)
c (Å)	10.7605 (3)	10.7792 (2)	10.7873 (3)
α (deg)	99.85 (1)	99.956 (3)	100.01 (1)
β (deg)	118.20 (1)	118.080 (4)	118.36 (1)
γ (deg)	111.37 (1)	111.191 (4)	110.56 (1)
vol. (Å^3)	217.8	215.8	214.6
fiber-axis direction vector			
a	0.0752 (2)	0.0506 (1)	0.0438 (1)
b	0.0813 (2)	0.0403 (1)	0.0336 (1)
c	1	1	1
tilting angle (deg)	6.32	3.70	3.16
disorientation[a] (deg)	5.72 (1)	3.900 (3)	3.05 (3)
crystallite size			
$L_1 = L_2$ (Å), lateral	63.5 (1)	80.4 (1)	72.2 (1)
L_3 (Å), axial	76.6 (1)	86.4 (1)	108.6 (1)
paracrystallinity[b] (Å^2)			
$T_{11} = T_{22} = T_{12} = T_{21}$	−0.0454 (2)	−0.0188 (1)	−0.0178 (1)
$T_{31} = T_{32}$	−0.0748 (7)	−0.0258 (3)	−0.0356 (3)
$T_{13} = T_{23}$	0.0341 (1)	−0.0626 (4)	0.1073 (2)
T_{33}	0.01290 (2)	0.0121 (1)	−0.0262 (1)
R_1[c]	1.616	2.781	2.640
R_2[d]	0.137	0.201	0.191
NV[e]	20	31	31

[a] σ for the angular distribution $\exp(-\theta^2/2\sigma^2)$. [b] See ref 23. [c] Calculated using $R_1 = [[\sum_{i=1}^{NO}\omega_i(I_{io} - I_{ic})^2]/(NO - NC)]^{1/2}$ in which weighting scheme $\omega = 1/\sigma(C)^2$ and $\sigma(C)^2 = C + 0.0001C^2$. [d] Calculated using $R_2 = [[\sum_{i=1}^{NO}\omega_i(I_{io} - I_{ic})^2]/(NO - NC)]^{1/2}$. [e] NV = number of variables.

number of reflections. In this study the consistency between the observed and the calculated patterns and the reasonableness of the structural model are more important in the judgement of the success of the refinement.

The estimated standard deviations (esd's) for the variables of this study are very small. The accuracy of the variables cannot be estimated by the rule-of-three-esd's, although this three-esd-rule is widely used in most other crystallographic studies of integrated intensity refinement. It has been known for some time that the esd's are systematically underestimated in the Rietveld refinement.[26,27] In profile refinement each reflection peak consists of many points. The number of observations is much larger than the number of parameters; however, the observations which belong to the same reflection are correlated. Therefore, the esd's are usually underestimated with profile refinement. Several methods have been developed to overcome this problem.[28-30] It should be pointed out that in a fiber diffraction study the esd's also depend on the background correction since the observations depend on how much background is removed from the original diffraction pattern.

The dimensions of the unit cell change with heat treatment. From PET4 to PET4B the lengths of the a and b axes decrease, but the length of the c axis increases. A similar relation between the unit-cell axes of PET fiber crystallites and the processes of annealing and tension during annealing has been reported earlier.[31] However, the accuracy of the earlier study is limited since in this study the unit-cell angles are treated as constants and the lengths of the axes are determined from the positions of only three reflections (010, 100, and $\bar{1}05$). The systematic change of the dimension of the unit cell of PET fibers with the draw ratio has also been reported.[32] Since the PET fiber crystallites grow far from equilibrium, internal strain may be produced in fibers during the manufacturing process. The strain can cause the change in the molecular conformation and even in bond lengths and angles[33] and

Table II
Atomic Coordinates and Temperature Factors (Å^2)[a]

The temperature factor of C atom B = 3.11 (1), for PET4
= 3.52 (1), for PET4A
= 3.53 (1), for PET4B

atom	x	y	z
O1	0.098 51	0.039 30	0.190 09
	0.088 74	0.028 31	0.187 39
	0.084 89	0.027 91	0.186 54
O2	−0.037 57	−0.372 10	0.177 25
	0.097 37	−0.393 88	0.164 30
	−0.086 44	−0.393 14	0.167 40
C1	0.138 87	−0.010 83	0.066 48
	0.121 35	−0.027 59	0.061 25
	0.122 60	−0.027 67	0.062 53
C2	0.019 74	−0.154 65	0.237 25
	−0.011 29	−0.169 00	0.230 23
	−0.007 61	−0.168 49	0.231 45
C3	0.009 55	−0.074 80	0.372 97
	−0.005 46	−0.081 69	0.369 67
	−0.003 68	−0.081 49	0.370 11
C4	−0.053 78	−0.248 46	0.441 08
	−0.102 75	−0.261 69	0.430 42
	−0.105 14	−0.262 31	0.429 85
C5	0.063 92	0.175 13	0.430 98
	0.097 72	0.180 58	0.438 56
	0.102 39	0.182 34	0.439 48
H1	0.104 59	−0.182 89	0.035 24
	0.051 01	−0.208 85	0.021 54
	0.055 86	−0.208 95	0.023 78
H2	0.395 20	0.110 35	0.101 92
	0.385 31	0.075 17	0.097 30
	0.386 90	0.075 41	0.099 73
H3	−0.090 73	−0.418 99	0.400 83
	−0.173 04	−0.440 70	0.382 86
	−0.177 34	−0.442 34	0.381 89
H4	0.107 07	0.292 86	0.383 85
	0.163 95	0.302 75	0.396 55
	0.171 40	0.304 90	0.398 06

[a] Coordinates are in fractions of the a, b, and c parameters of Table I. The results of refinement of PET4 (top line) are followed by those of PET4A and PET4B.

Table III
Bond Lengths (Å), Bond Angles (deg), and Conformation Angles (deg)

	PET4	PET4A	PET4B	DBB[b]
C1–C1′	1.462	1.449 (2)	1.462 (2)	1.471
C1–O1	1.424	1.431 (1)	1.424 (2)	1.446
O1–C2	1.338	1.337 (1)	1.338 (2)	1.351
C2–O2	1.212	1.212 (1)	1.212 (2)	1.260
C2–C3	1.484	1.486 (1)	1.484 (2)	1.480
C3–C4	1.39	1.39	1.39	1.406
C3–C5	1.39	1.39	1.39	1.331
C4–C5′	1.39	1.39	1.39	1.361
C1′–C1–O1	111.7	111.7 (1)	111.7 (1)	104.9
C1–O1–C2	117.0	117.1 (1)	117.0 (1)	114.4
O1–C2–O2	124.5	124.4	124.5	121.9
O1–C2–C3	112.4	112.2 (1)	112.4 (1)	110.1
O2–C2–C3	123.0	123.3 (1)	123.0 (1)	127.0
C2–C3–C4	120	120.1 (1)	120.2 (1)	117.4
C2–C3–C5	120	119.6 (1)	119.3 (1)	125.6
C4–C3–C5	120	120	120	116.9
C3–C4–C5′	120	120	120	120.0
C3–C5–C4′	120	120	120	122.9
C2–O1–C1–C1′	121.3 (1)	124.9 (1)	126.0 (1)	158.7
C3–C2–O1–C1	176.2	175.5	174.9	−178.2
C4–C3–C2–O1	182.4 (1)	179.9 (1)	177.9 (1)	169.2
ψ	−5.3 (1)	−13.7 (1)	−13.8 (1)	

[a] Standard errors are given for the independent variables; other parameters are derived or assumed. [b] Calculated from the coordinates provided in ref 7.

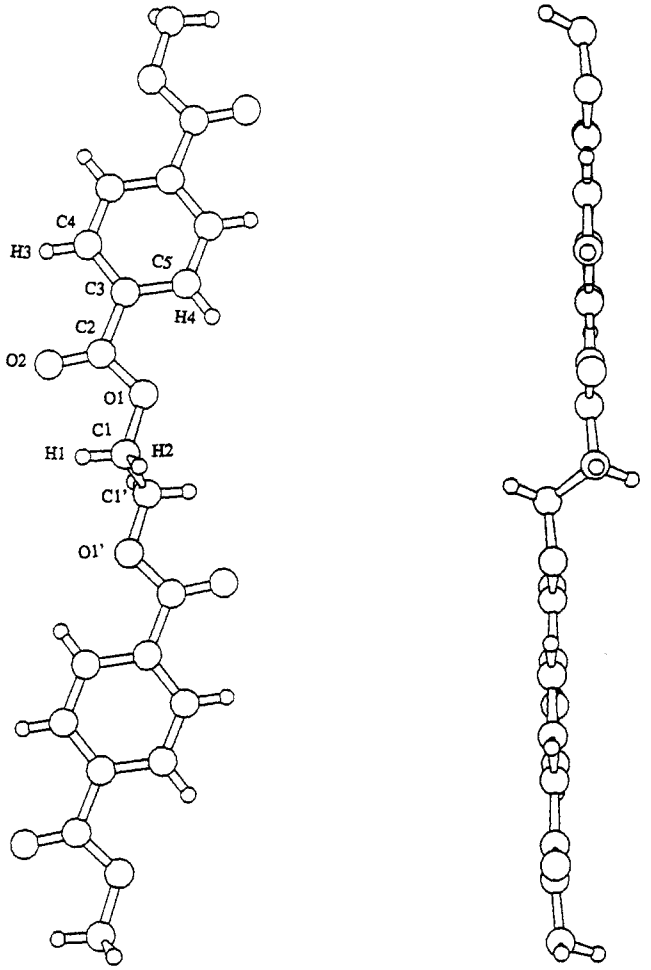

Figure 3. Molecular conformation of PET4B with the atom-numbering scheme.

in turn can affect the dimensions of the unit cell. Therefore, there is no universal unit-cell parameters which can fit all crystallites of PET fibers prepared with different procedures. It should be pointed out that the unit-cell parameters of PET fibers are difficult to determine accurately with the traditional fiber diffraction method. Eight parameters have to be determined because of the $P\bar{1}$ space group and the presence of a tilting angle between the c axis of the crystallites and the fiber axis. Usually it is difficult to have enough strong and isolated reflections to determine the eight parameters. Additional sources of error unique to the film method[13] add to the difficulty of the determination of the unit-cell parameters.

The molecular conformation angles and the molecular orientation angle are sensitive to the heat treatment. The conformation angles are significantly different from DBB's results,[7] even though our refinement started with DBB's values. The conformation angle, C2–O1–C1–C1′, is more than 30° less than DBB's value. This angle shows a tendency to increase, but the other two conformation angles, C4–C3–O2–C2 and C3–O2–C2–C1, show a tendency to decrease from PET4 to PET4B. The terephthaloyl unit is approximately planar. The bond lengths and bond angles obtained from this study are all among reasonable ranges. The bond length values, except those of the C–C bonds of the phenylene ring, agree with DBB's results. The bond angle of C1′–C1–O1 (about 111.7°) is quite different from DBB's value (104.9°). Comparing Figure 4 with the corresponding Figure 7 in DBB's paper, the positions of the hydrogen atoms of ethylene glycol are considerably different because of the different conformation of the molecule. The packing contacts of the C and O atoms are not signficantly affected by the change in molecular conformation. The shortest interchain distances in PET4B are within acceptable limits (C–C, 3.60 Å; O–C, 3.62 Å; O–O, 3.30 Å).

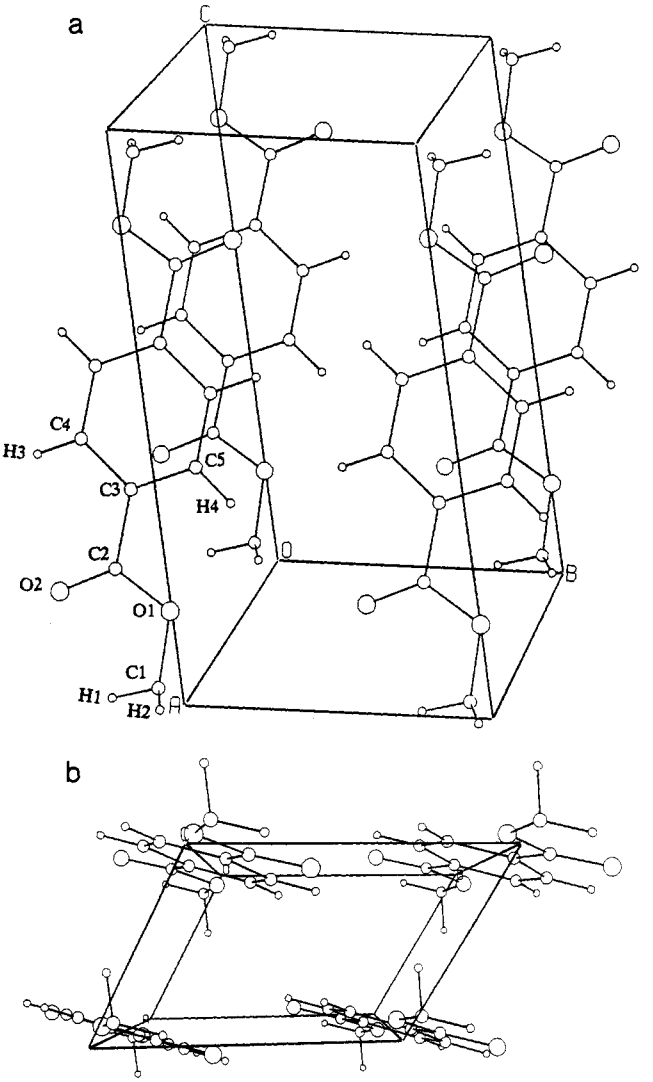

Figure 4. Position of the molecular chains in the unit cell of PET4B: (a) projection normal to the 010 plane; (b) projection along the c axis.

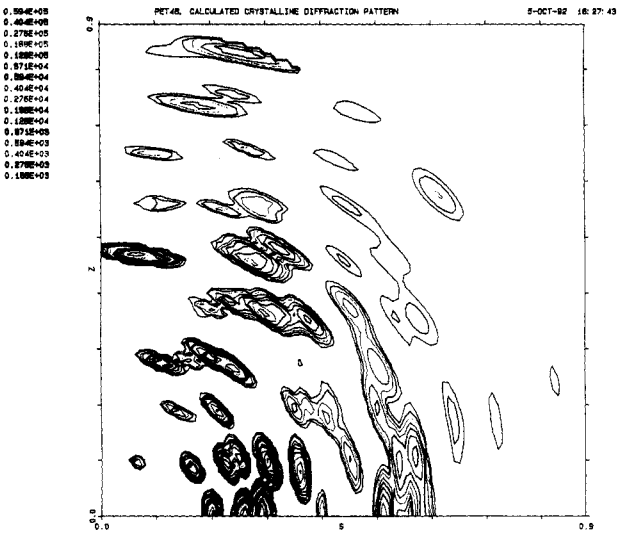

Figure 5. Contour plot of the calculated crystalline diffraction intensity of PET4B. The interval of the contours is $(0.1)^{1/6}$ of the value of the previous contour line.

The crystallites of the PET fibers grow bigger in all directions with annealing. Adding tension during annealing causes the crystallites to grow preferentially along the direction of the applied force, but the volume of the crystallites does not increase significantly with the application of tension. The ratio of the volumes of the crystallites is 0.55/0.99/1.0 for PET4/PET4A/PET4B. The volume ratio agrees with the ratio of the crystallinities 0.56/0.96/1.0 based on DSC measurement.[34] The thus determined crystallinities are 28, 48, and 50% respectively for PET4, PET4A, and PET4B. The crystallites in all of these PET samples are elongated along the fiber axis. The anisotropy of the shape of the crystallites is consistent with the shape of the crystallites of hydrolyzed PET4B samples visualized by the AFM technique.[35] The lengths of the crystallites of PET4A (86.4 Å) and PET4B (108.6 Å) fit well with the long period spaces of 120 Å measured by the SAXS technique.[35] No SAXS diffraction peak is observed for the PET4 sample. Low crystallinity, the small size of the crystallites, and the large unit-cell volume of PET4 all make the electron density difference between the crystalline and amorphous regions not great enough to produce any diffraction peak in SAXS.

In PET fibers the crystalline c axis may differ from the fiber axis. The tilting of the crystallites makes the reflections shift away from their layer line. The coordinates (s_i,z_i) of a reflection in the two-dimensional fiber diffraction pattern are

$$z_i = \mathbf{H}_i\mathbf{T} \tag{1}$$

$$s_i = (d_i^2 - z_i^2)^{1/2} \tag{2}$$

where $\mathbf{H}_i$ is the reflection position vector in the reciprocal lattice crystal Cartesian system, $\mathbf{T}$ is the unit vector of the fiber-axis direction, and d_i is the length of the reflection position vector. The tilting angle is suggested to be caused by the internal strains developed during crystallization.[36] The crystal modulus is reported to increase systematically with the decrease of the tilting angle.[37] The annealing, particularly under tension, reduces the tilting angle. These treatments also reduce the disorientation (mosaic angle) of the crystallites. The tilting and disorientation can be converted to an orientation function[5,38] which is often used as an important parameter in fiber structure studies. The orientation functions are 0.936, 0.974, and 0.983 for PET4, PET4A, and PET4B, respectively. The decrease of the tilting angle and disorientation is indicative of the decrease of the internal strains. The reduction of the shrinkage rate from 17% of PET4 to 2% of PET4B[34] may reflect this decrease of the internal strain.

In Figure 1 the peaks that are far away from the center of reciprocal space are broader than the peaks near the center. Such propagative broadening of reflection peaks cannot be explained solely by the small size of crystallites. Figure 6 is the calculated pattern in which the crystal structure is the same as in Figure 5, but the paracrystallinity matrix is set as zero. The peaks in the high-scattering angle region are too sharp and too strong, while the peaks in the low-scattering angle region can still be fitted relatively well by adjusting the crystallite size and other parameters. The propagative peak width increase should be caused by other defects in the crystallites. It is hard to determine each of these defects experimentally. A paracrystallinity matrix[23] is included in FIBLS to account for this propagative peak width increase. The formula for the reflection peak width (in an orthogonal system and before cylindric convolution) is

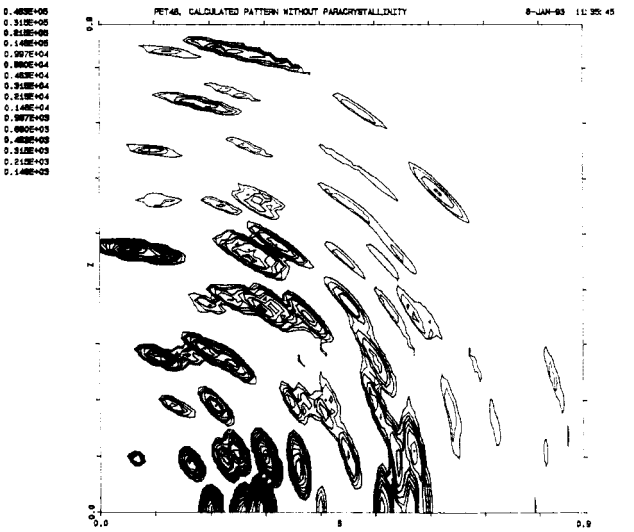

Figure 6. Contour plot of the calculated crystalline diffraction intensity with the same crystal structure as Figure 5 but with a paracrystallinity matrix of zero. The interval of the contours is $(0.1)^{1/6}$ of the value of the previous contour line.

$$G(b_i) = \frac{1}{\sigma_i(2\pi)^{1/2}}\exp\left(-\frac{\Delta b_i^2}{2\sigma_i}\right) = \left(\frac{a_{ii}}{\pi}\right)^{1/2}\exp(-a_{ii}\Delta b_i^2) \tag{3}$$

where

$$a_{ii} = \frac{1}{\left[\pi^3|A_i|^2(\mathbf{b}_h\mathbf{T}_i\mathbf{b}_h)^2 + \frac{1}{\pi L_i^2}\right]} \tag{4}$$

where A_i = mean reciprocal lattice edge, L_i = crystallite size along axis i, $\mathbf{b}_h$ = a reciprocal lattice vector, and $\mathbf{T}_i$ = the paracrystallinity[23] along axis i. If the paracrystallinity is zero, the above formula is equivalent to the Scherrer equation.[39] It should be noted that Hosemann's paracrystallinity function is used to explain the peak broadening caused by all the other defects. A different paracrystallinity model has been proposed;[40] however, it is hard to determine which model suits this kind of application better because of the lack of high-angle strong reflection peaks and the complicated background scattering.

As it has been mentioned, the success of the interpretation of a fiber diffraction pattern depends largely on the separation of the background. Caution must be taken when using the Fourier filter method to avoid introduction of errors into the observations by the background removal. The range of the modifying function should not be overly large, especially in the initial cycles of background removal. In this study the type and the parameters of the modifying function are decided totally according to experience. It is hoped that a better modifying function will be found in the future and that the parameters of the modifying function can be included in the refinement in order to reduce the number of background correction cycles and to reduce the time required for the refinement.

Both crystalline and amorphous phases play an important role in the mechanical and thermal properties of fibers. The amorphous scattering and crystalline diffraction are inevitably mixed together in the observed fiber diffraction patterns. This full-pattern refinement fits the crystalline diffraction well. The next step in this study is to analyze the amorphous scattering by removing the crystalline diffraction from the observed diffraction patterns, a topic to be described in a future publication.

Acknowledgment. Y.F. is grateful to G.-Y. Chen for providing the sample and information about its manufacturing process and properties. Thanks are also due to B. Annis and J. D. Londono for helpful discussions. This work was supported by the Division of Materials Research, National Science Foundation, Polymers Program, under Grant DMR 92-00520, and the Division of Materials Sciences, Office of Basic Energy Sciences, U.S. Department of Energy, under Contract DE-AC05-84OR21400 with Martin Marietta Energy Systems, Inc.

References and Notes

(1) Immirzi, A.; Iannelli, P. *Gazz. Chim. Ital.* **1987**, *117*, 201.
(2) Immirzi, A.; Iannelli, P. *Macromolecules* **1988**, *21*, 768.
(3) Iannelli, P.; Immirzi, A. *Macromolecules* **1989**, *22*, 196.
(4) Iannelli, P.; Immirzi, A. *Macromolecules* **1990**, *23*, 2375.
(5) Busing, W. R. *Macromolecules* **1990**, *23*, 4608.
(6) Busing, W. R. Annual Meeting of the American Crystallographic Association, Toledo, OH, July 1991.
(7) Daubeny, R. P.; Bunn, C. W.; Brown, C. J. *Proc. R. Soc. London* **1954**, *226A*, 531.
(8) Kilian, H. G.; Halboth, H.; Jenckel, E. *Kolloid Z.* **1960**, *172*, 166.
(9) Tomashpol'skii, Y. Y.; Markova, G. S. *Polym. Sci. USSR. (Engl. Transl.)* **1964**, *6*, 316.
(10) Fakirov, S.; Fisher, E. W.; Schmidt, G. F. *Makromol. Chem.* **1975**, *176*, 2459.
(11) Kinoshita, Y.; Nakamura, R.; Kitana, Y.; Ashida, T. *Polym. Prepr. (Am. Chem. Soc., Div. Polym. Chem.)* **1979**, *20*, 454.
(12) Bornschlegl, E.; Bonart, R. *Colloid Polym. Sci.* **1980**, *258*, 319.
(13) Hall, H. *Structure of Crystalline Polymers*; Elsevier Applied Science Publishers: London and New York, 1984; Chapter 2.
(14) Fibers provided by Dr. G.-Y. Chen, Allied-Signal, Inc., Technical Center, Petersburg, VA. For additional information on the fibers, see: Chen, G.-Y.; Cuculo, J. A.; Tucker, P. A. *J. Appl. Polym. Sci.* **1992**, *44*, 447.
(15) Dorset, D. L.; Hu, H.; Jäger, J. *Acta Crystallogr.* **1991**, *A47*, 543.
(16) Prevorsek, D. C. *J. Polym. Sci.* **1971**, *32*, 343.
(17) Fischer, E. W.; Fakirov, S. *J. Mater. Sci.* **1976**, *11*, 1041.
(18) Lee, S.; Miyaji, H.; Geil, P. H. *J. Macromol. Sci.* **1983**, *B22*, 489.
(19) Aharoni, S. M.; Sharma, R. K.; Szobota, J. S.; Vernick, D. A. *J. Appl. Polym. Sci.* **1983**, *28*, 2177.
(20) Murthy, N. S.; Correal, S. T.; Minor, H. *Macromolecules* **1991**, *24*, 1185.
(21) Richardson, J. W., Jr.; Faber, J., Jr. *Advances in X-ray Analysis*; Barret, C. S., et al., Eds.; Plenum: New York, 1986; Vol. 29, p 143.
(22) One-dimensional Tukey function:

$$T = \begin{cases} 1, & \text{for } r < r_1 \\ 0, & \text{for } r > r_2 \\ 0.5 + 0.5 \cos\left[\dfrac{\pi(r - r_1)}{r_2 - r_1}\right], & \text{for } r_1 < r < r_2 \end{cases}$$

where $r = s/\Delta s$ and s is the distance to the meridian axis in direct space. The Δs, r_1, and r_2 are adjustable parameters.
(23) Hosemann, R.; Bagchi, S. N. *Direct Analysis of Diffraction by Matter*; Interscience: New York, 1962; Chapter IX.
(24) Brisse, F.; Pérez, S. *Acta. Crystallogr.* **1976**, *B32*, 2110.
(25) Pérez, S.; Brisse, F. *Can. J. Chem.* **1975**, *53*, 3551.
(26) Sakata, M.; Cooper, M. J. *J. Appl. Crystallogr.* **1979**, *12*, 554.
(27) Young, R. A. *Natl. Bur. Stand. (U.S.), Spec. Publ.* **1979**, *No. 567*, 143.
(28) Pawley, G. S. *J. Appl. Crystallogr.* **1980**, *13*, 630.
(29) Scott, H. G. *J. Appl. Crystallogr.* **1983**, *16*, 159.
(30) Bérar, J.-F.; Lelann, P. *J. Appl. Crystallogr.* **1991**, *24*, 1.
(31) Huisman, R.; Heuvel, H. M. *J. Appl. Polym. Sci.* **1978**, *22*, 943.
(32) Sun, T.; Zhang, A.; Li, F. M.; Porter, R. S. *Polymer* **1988**, *29*, 2115.
(33) Tadokoro, H. *Polymer* **1984**, *30*, 147.
(34) Jin, Y.; et al. Manuscript in preparation.
(35) Annis, B.; et al. Manuscript in preparation.
(36) Asano, T.; Seto, T. *Polym. J.* **1973**, *5*, 72.
(37) Thistlethwaite, T.; Jakeways, R.; Ward, T. M. *Polymer* **1988**, *29*, 61.
(38) Alexander, L. E. *X-ray Diffraction Methods in Polymer Science*; Wiley: New York, 1969; p 241.
(39) Warren, B. E. *X-ray Diffraction*; Addison-Wesley: Reading, MA, 1969; pp 252–253.
(40) Blöchl, G.; Bonart, R. *Makromol. Chem.* **1986**, *187*, 1525.